BOREAS An international journal of Quaternary research

Palaeoenvironmental changes recorded at the Velika Vrbica loess-palaeosol sequence, Wallachian Basin, during MIS 3–MIS 1

ZORAN M. PERIĆ, CATHAL S. RYAN, WARREN THOMPSON, MILICA G. RADAKOVIĆ, PETAR KRSMANOVIĆ, HELENA ALEXANDERSON AND SLOBODAN B. MARKOVIĆ

BOREAS

Perić, Z. M., Ryan, C. S., Thompson, W., Radaković, M. G., Krsmanović, P., Alexanderson, H. & Marković, S. B.: Palaeoenvironmental changes recorded at the Velika Vrbica loess-palaeosol sequence, Wallachian Basin, during MIS 3–MIS 1. *Boreas*. https://doi.org/10.1111/bor.70009. ISSN 0300-9483.

This study presents a detailed investigation of the Velika Vrbica loess-palaeosol sequence, situated in the Wallachian Basin of northeastern Serbia, with the aim to reconstruct palaeoenvironmental changes spanning Marine Isotope Stages (MIS) 3 to 1. Using optically stimulated luminescence (OSL) dating, low field magnetic susceptibility (χ_{lf}), and mass accumulation rates (MARs), we have developed a robust geochronological framework and analysed sedimentary and environmental processes over the last glacial–interglacial cycle. The OSL chronology reveals consistent loess deposition from ~41 to 3 ka, with peak accumulation rates recorded during MIS 3 and late MIS 2. The MAR data challenge conventional models of loess formation, as higher deposition rates are observed during the interstadial MIS 3 compared to the Last Glacial Maximum. This finding suggests regional variations in aeolian activity and climate dynamics that differ from the widely accepted pattern of intensified dust deposition during colder glacial periods. The environmental magnetic record of the Velika Vrbica loess sequence presented here shows more similarities with equivalent sections in the Wallachian Basin than in the Vojvodina region. These findings contribute to the broader understanding of loess formation processes and palaeoenvironmental variability on a continental scale, reinforcing the importance of high-resolution chronological and sedimentological studies in disentangling global vs. regional influences on past dust deposition.

Zoran M. Perić (zoran.peric@geol.lu.se) and Helena Alexanderson, Department of Geology, Lund University, Sölvegatan 12, SE-223 62 Lund, Sweden; Cathal S. Ryan, Irish Climate Analysis and Research Units, Department of Geography, Maynooth University, Co. Kildare, Maynooth, Ireland; Warren Thompson, Technical University of Denmark, Risø Campus, Frederiksborgvej 399 – Building 201, 4000 Roskilde, Denmark; Milica G. Radaković and Petar Krsmanović, Department of Geography, Tourism and Hotel Management, Faculty of Science, University of Novi Sad, Trg Dositeja Obradovića 3, 21000 Novi Sad, Serbia; Slobodan B. Marković, Division of Geochronology and Environmental Isotopes, Institute of Physics – Centre for Science and Education, Silesian University of Technology, Konarskiego 22B, Gliwice 44-100, Poland, Serbian Academy of Sciences and Arts, Knez Mihajlova 35, 11000 Belgrade, Serbia and University of Montenegro, Cetinjska 2, 81000 Podgorica, Montenegro; *received 12th December 2024, accepted 31st March 2025.*

Loess-palaeosol sequences (LPSs) are among the most valuable terrestrial archives of Quaternary palaeoenvironmental change. These sedimentary records, composed of alternating loess layers and palaeosols, provide insights into glacial and interglacial cycles, that reflect shifts in climate, vegetation, and sedimentation patterns (Schaetzl *et al*. 2018). Through detailed stratigraphical and geochronological analyses, LPSs enable the reconstruction of regional climate histories and their linkage to global climatic events (Marković *et al*. 2015). The Wallachian Basin, located in southeastern Europe, is one of the most significant loess deposition regions globally, preserving extensive and relatively undisturbed sequences spanning the Quaternary (Jordanova *et al*. 2022a, b). The Velika Vrbica LPS, situated on the southwestern bank of the Danube River in northeastern Serbia and marks the westernmost boundary of the Wallachian Basin. This site is particularly well suited for studying palaeoenvironmental dynamics due to its strategic location near the Danube River and the Iron Gates Gorge, a region shaped by complex geomorphological and climatic processes. While LPS studies across Europe often emphasize glacial maxima as periods of intensified aeolian dust deposition, the Velika Vrbica LPS presents an opportunity to evaluate whether this paradigm holds true for southeastern Europe. In particular, previous studies have noted discrepancies in dust accumulation patterns for this region (Perić *et al*. 2020, 2022a, 2024; Marković *et al*. 2021), with higher rates observed during warmer interstadial phases, contradicting established models. This study aims to investigate such patterns by integrating optically stimulated luminescence (OSL) dating, low field magnetic susceptibility (χ_{lf}), and mass accumulation rate (MAR) data. By combining high-resolution geochronological data with sedimentological and palaeoclimatic analyses, this research contributes to advancing our understanding of the interplay between global climate systems and regional environmental responses. It also highlights the role of southeastern European LPSs in refining models of loess formation and dust dynamics, with implications for reconstructing past climate variability and predicting future changes in similar semi-arid environments.

DOI 10.1111/bor.70009

Geological background and site description

During the Cretaceous and Palaeogene, the collision between the African and Eurasian plates triggered significant geological and geomorphological transformations in southeastern Europe. At the time, the Tethys Sea separated the two continental landmasses. As the Alpine orogeny progressed, the convergence of these major plates caused compression and extension of smaller microplates, leading to the gradual closure of the Tethys Sea. This tectonic activity reworked the continental crust, giving rise to basins and mountain chains. The formation of the Carpathian Mountains ultimately divided the Paratethys Sea, shaping what would later become the Carpathian (Pannonian) and Wallachian (Pontian) basins (Marković *et al.* 2016). Towards the east of the Wallachian basin (modern-day eastern Romania), further compression and uplift resulted in the creation of the Dobrogea Plateau. This affected the flow direction of the Danube and diverted the river northwards. The redirection of the Danube and the tectonic altering of the region have culminated in a landscape where conditions for loess deposition and accumulation are extremely favourable. Thus, the widespread accumulation of loess and loess-like sediment has produced the most extensive and complete terrestrial archives of palaeoclimatic and environmental changes in Europe during the Quaternary (Lehmkuhl *et al.* 2021).

The Velika Vrbica LPS is situated in northeastern Serbia (latitude 44°35′1.70″N, longitude 22°43′15.97″E), 10 km east of the city Kladovo and ~20 km downstream of the Iron Gate gorge (Fig. 1). Positioned near the Danube River, it rises ~20 m above its southwestern bank, marking the westernmost boundary of the Wallachian Basin. This LPS is ~12 m thick, consisting of two fossil soils and two loess layers and is underlain by a fluvial terrace (Fig. 2).

The profile is analysed within the framework of the Danube loess stratigraphy (Marković *et al.* 2015). Two primary units, S0 (the current interglacial soil) and L1 (the last glacial composite loess), are distinguished in the uppermost 5 m. The uppermost unit, S0, is a 70-cm-thick modern Chernozem soil that transitions gradually into the underlying loess layer, L1. The complex L1 loess unit, approximately 8 m thick, is further subdivided: the upper subdivision, the L1LL1 loess subunit, is characterized by typical porous loess with a pale yellow coloration, extending from 0.7 to 4.15 m depth. Within this section, a ~1-m-thick aeolian sand layer is observed between 1.1 and 2.1 m. Beneath L1, the S1 palaeosol is found, approximately 2 m thick and characterized as a reddish-brown Chernozem-pedocomplex. Below S1 lies the penultimate loess unit, L2, with a basal thickness of 90 cm, exhibiting porous properties similar to those of L1. This study provides a comprehensive investigation of the uppermost 5 m of the profile, encompassing the stratigraphical sequence of the last glacial–interglacial cycle.

Material and methods

Sampling and facilities

Luminescence dating samples were collected from the upper 5 m of the LPS at 50-cm intervals using stainless steel tubes (20 cm in length, 5 cm in diameter) driven into a freshly cleaned profile. Sample preparation took place at the Lund Luminescence Laboratory, Lund University, Sweden, under low-intensity red light conditions. Approximately 2 cm of the outer material, potentially exposed to sunlight, was set aside for water content measurement and dose rate calculations. The remaining material from the core of each tube was wet sieved using 90 and 63 µm sieves to isolate specific grain-size fractions. Quartz was targeted for dating due to its abundance and proven suitability for luminescence analysis in this region (e.g. Perić *et al.* 2019, 2024). The extracted material underwent sequential chemical treatments to prepare the quartz fraction. Carbonates and fine organic matter were removed by treating the samples with 10% HCl for 60 min and 10% H_2O_2 for 60 min, respectively. To isolate quartz, the material was placed in a sodium heteropolytungstate solution (density 2.62 g cm^{-3}; LST 'Fastfloat') for 24 h. Quartz grains with a density greater than 2.62 g cm^{-3} were then exposed to 40% HF for 90 min to eliminate feldspar contamination, followed by a 10% HCl treatment for 120 min to dissolve any fluorides. The prepared quartz grains were mounted on stainless steel discs using silicone oil spray, with aliquot sizes of either 8 or 2 mm selected based on signal intensity. Luminescence measurements were conducted using Risø TL/OSL readers, model DA-20 (Bøtter-Jensen *et al.* 2003). The readers were equipped with blue LEDs (470 nm, ~80 mW cm^{-2}) and infrared (IR) LEDs (870 nm, ~135 mW cm^{-2}). Irradiation was performed using a ^{90}Sr/^{90}Y beta source, which was calibrated with the Risø calibration quartz, batch 123 (Hansen *et al.* 2015). Quartz OSL signals were collected through 7.5 mm of Schott U-340 (UV) glass filter. Data analysis was conducted using the Risø TL/OSL software (Duller 2015).

Dose rate measurements

The sediment for dose rate measurements (~100 g per sample) was dried, ground to <20 µm, and ignited for 24 h at 450 °C. Following this treatment, the samples were then taken to the Technical University of Denmark (DTU), Nordic Laboratory for Luminescence Research, for casting and high-resolution gamma spectrometry measurements. The samples were mixed with wax, cast in a fixed disc-shaped geometry to retain ^{222}Rn, and stored for >21 days to allow ^{222}Rn to build up to equilibrium with ^{226}Ra. Finally, the concentrations of ^{238}U, ^{232}Th and ^{40}K were determined by measuring the samples for >24 h on a high-resolution gamma spectrometer. The calibration of the spectrometers was conducted

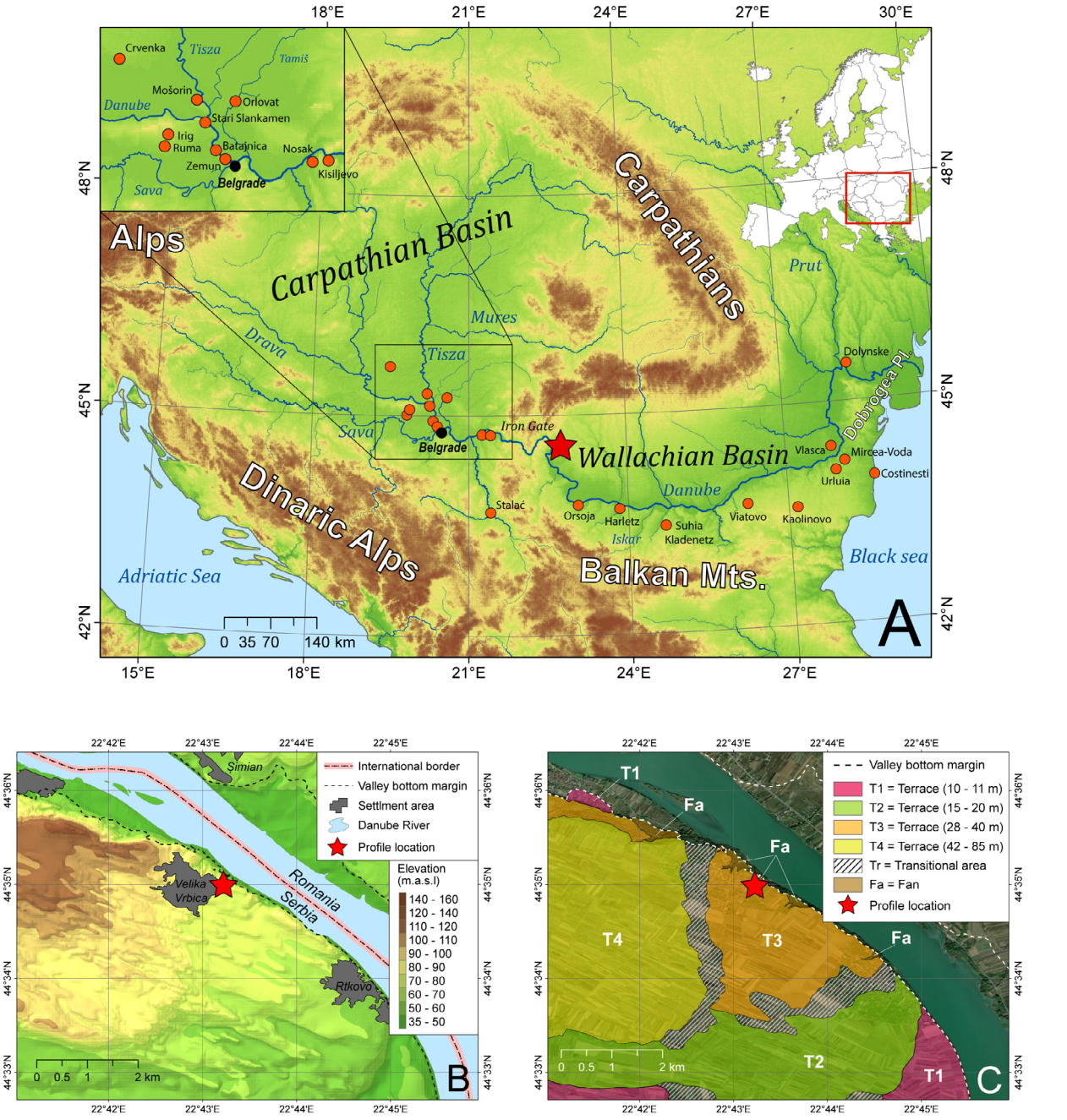

Fig. 1. A. Map of the Middle and Lower Danube Basins showing the position of the Velika Vrbica LPS (red star) and other key LPSs in the region (red circles) (Avramov *et al.* 2006; Marković *et al.* 2014, 2015; Obreht *et al.* 2015; Laag *et al.* 2021; Jordanova *et al.* 2022a, b; Perić *et al.* 2022a). The Middle and Lower Danube Basins are located within a complex tectonic setting shaped by the convergence of the Eurasian and African plates and regional microplate interactions. The core of the Middle Danube Basin is the Tisza Mega-unit, which underwent significant extension and subsidence during the Miocene, driven by back-arc tectonics. In contrast, the Lower Danube Basin is part of the Moesian Platform, a stable, Europe-derived unit. Between these regions lies the Carpathian thrust belt, formed during the Alpine orogeny as a result of subduction and collision processes (Schmid *et al.* 2020). B. The setting of the Velika Vrbica LPS. C. Geomorphological map of the area surrounding the Velika Vrbica LPS.

according to Murray *et al.* (2005) with conversion factors to calculate the dry dose rate provided by Guérin *et al.* (2011).

The water content was measured for each sample, although the values were exceptionally low, which is likely due to the longer profile exposure to air prior to sampling. Thus, we do not consider the measured water content to be a realistic estimate over the burial time. Instead, the water content is assumed to be 15±5%, an assumption based on previous studies within the Danube basin (Antoine *et al.* 2009; Schmidt *et al.* 2010; Perić *et al.* 2019, 2022a). The alpha and beta attenuation fac-

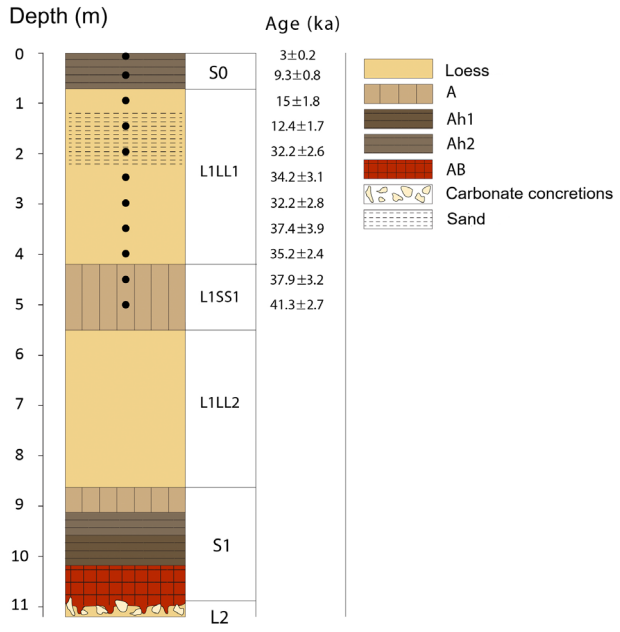

Fig. 2. Lithology of the Velika Vrbica LPS, position of the luminescence samples (full black circles) together with the OSL ages. A = initial pedogenetic horizon; Ah1 = strongly developed humic horizon; Ah2 = humic horizon; AB = transitional horizon between initial pedogenesis and background sediment.

tors were calculated based on the methods of Brennan *et al.* (1991) and Guérin *et al.* (2012), respectively, while the dose rate conversion factors were derived from Guérin *et al.* (2011). Contributions from cosmic rays were calculated using depth, altitude, density, latitude and longitude for each sample with an assumed uncertainty of 10% (Prescott & Hutton 1994). Final ages were calculated using the DRAC dose rate and age calculator, version 1.2 (Durcan *et al.* 2015) and the resulting radionuclide concentrations are summarized in Table 1.

Equivalent doses

Before measuring the equivalent dose (D_e), the purity of quartz grains and potential feldspar contamination were evaluated through initial IR depletion tests conducted on three aliquots per sample. The procedure involved preheating the samples to 220 °C for 10 s, followed by optical stimulation with IR LEDs at 125 °C for 100 s and with blue LEDs at 125 °C for 40 s. These steps were used to measure luminescence signals from feldspar and quartz, respectively. Feldspar contribution to the OSL signal was quantified by calculating the ratio of the IR-stimulated signal to the blue-stimulated signal (IR/B ratio). Among the 10 samples analysed, four exhibited depletion ratio values exceeding 10% (Table S1). Based on these results, two approaches were applied for D_e determination in the Velika Vrbica quartz samples. The single aliquot regenerative dose (SAR) protocol was implemented for samples with an IR/B ratio below 10% (Murray & Wintle 2000, 2003). Quartz grains were measured using preheat and cut-heat temperatures of 240 and 200 °C, respectively, with the rationale for these settings detailed below. Optical stimulation was carried out at 125 °C for 40 s using blue LEDs. The luminescence signal of interest was extracted from the initial 0.16 s of the decay curve, with background subtraction performed using the signal from the 0.32–0.48 s interval. Sensitivity adjustments were made based on the OSL response to a test dose, which was approximately 10% of the estimated natural dose for all measurements. Each SAR cycle concluded with a high-temperature bleach at 280 °C for 40 s (Murray & Wintle 2003). Intrinsic tests, such as recycling and recuperation, were included in each measurement following the SAR protocol (Murray & Wintle 2003). A tolerance of up to 10% deviation from unity was applied for recycling ratio tests, while a recuperation signal within 5% of the natural signal was deemed acceptable. Aliquots failing to meet these criteria were excluded from D_e calculations. For samples with an IR/B ratio exceeding 10% in the initial IR depletion tests, the double-SAR protocol was employed (Roberts & Wintle 2001). Results of the intrinsic tests are displayed in Fig. S1. The measurement sequence followed the SAR protocol but incorporated an additional stimulation step using IR LEDs at 125 °C for 100 s before optical stimulation with blue LEDs at 125 °C. This step ensured monitoring and depletion of the IRSL signal from feldspars. All luminescence data were processed using Risø Analyst software, version 4.57 (Duller 2015). Age calculations were performed with the DRAC Dose Rate and Age Calculator v. 1.2 (Durcan *et al.* 2015). The calculated D_e values, OSL ages, and dose rates are summarized in Table 1.

Magnetic susceptibility measurements

For the χ_{lf} measurements, 100 samples were collected at 5-cm intervals. The sediment was ground, packed in non-magnetic cubes (7 cm^3), and processed in the Palaeomagnetic laboratory, Lund University, Sweden. All measurements employed an AGICO Kappabridge MFK2 instrument and were subsequently analysed via the SAFYR7 software. During measurement, the applied field (A m^{-1}) and frequency (Hz) were 200 A m^{-1} and 976 Hz, respectively. When measuring the χ_{lf} of the sample, the volume of the non-magnetic cube was used. The mean mass of the loess was 0.0105 kg, and conversion of volume to mass was conducted according to the equation:

$$\frac{(\kappa)(v)}{m} = \chi \quad (1)$$

where the magnetic susceptibility (κ) of each sample is multiplied by the volume (v) and divided by the mass (m). This gives the magnetic susceptibility in mass as:

Table 1. A summary of sample codes, depth ranges, stratigraphical units, radionuclide concentrations, weighted mean D_e values, total dose rates, OSL ages, and associated errors in ka for the Velika Vrbica LPS. The parameter *n* indicates the count of accepted aliquots, and errors are expressed as one standard error of the mean.

Sample ID	Depth (cm)	Unit	^{238}U (Bq kg^{-1})	^{226}Ra (Bq kg^{-1})	^{232}Th (Bq kg^{-1})	^{40}K (Bq kg^{-1})	*n*	D_e (Gy)	Dose rate (Gy ka^{-1})	Age (ka)
22172	10	S0	22.73±3.97	37.42±0.7	42.49±0.65	457±11	31	7.6±04	2.5±0.1	3.0±0.2
22173	50	S0	24.30±9.41	32.09±0.89	38.08±0.88	390±16	20	21.1±1.2	2.3±0.1	9.3±0.8
22174	100	L1LL1	20.64±4.17	23.00±0.71	27.52±0.64	354±11	17	28.8±3.2	1.9±0.1	15.0±1.8
22175	150	L1LL1	20.66±9.32	24.89±0.85	29.87±0.85	344±15	28	23.8±2.7	1.9±0.1	12.4±1.7
22176	200	L1LL1	29.43±7.99	20.98±0.72	25.63±0.72	311±13	14	61.0±3.1	1.9±0.1	32.2±2.6
22177	250	L1LL1	32.81±10.92	33.51±1.01	38.07±1.01	418±18	22	82.6±4.9	2.4±0.2	34.2±3.1
22178	300	L1LL1	31.32±10.53	39.40±1.01	42.16±0.98	469±18	21	83.2±5.0	2.6±0.2	32.2±2.8
22179	350	L1LL1	32.65±9.84	26.28±0.93	41.93±0.93	437±16	14	93.7±8.1	2.5±0.1	37.4±3.9
22180	400	L1LL1	37.28±10.38	39.53±0.99	43.83±0.97	482±18	17	96.1±3.3	2.7±0.2	35.2±2.4
22181	450	L1SS1	20.84±11.26	45.43±1.11	47.74±1.07	540±20	23	101.7±5.6	2.7±0.2	37.9±3.2
22182	500	L1SS1	38.01±6.89	44.79±0.67	52.24±0.68	566±12	24	128.1±6.1	3.1±0.1	41.3±2.7

$$\chi = \chi 10^{-8} \quad (2)$$

The AGICO Kappabridge measures magnetic susceptibility at three operating frequencies and variable field ranges (Pokorný *et al*. 2011; Hrouda & Ježek 2014). At a frequency of 976 Hz, a field range of 2 to 700 A m^{-1} is specified, and when the susceptibility is higher than 5×10^{-5}, the error margin is between 0.1–0.2% when a field of 200 A m^{-1} is applied (Hrouda & Pokorný 2011). In several southeastern European loess studies (Constantin *et al*. 2019; Jordanova *et al*. 2022a), the two most commonly working frequencies are: 976 Hz (low frequency) and 15 616 Hz (high frequency) with a magnetic field of 200 A m^{-1}. However, in order to investigate the quantitative value representing the loess samples' bulk density, in this study, we used 976 Hz and 200 A m^{-1}. Still, it should be noted that issues may arise if viscous relaxation is the sole process and there are no influencing electrical eddy currents or weak field hysteresis (Hrouda *et al*. 2013). To avoid such issues, empty non-magnetic cubes were measured using the AGICO Kappabridge and SAFYR7 software to verify whether there were any influencing electrical eddy currents or weak field hysteresis that might affect the results of the loess samples.

Age-depth modelling and dust mass accumulation rates

The calculated OSL ages enabled the construction of a robust, continuous age-depth model. This investigation utilized the Bayesian age-depth modelling approach using the r.bacon code, version 3.00 (Blaauw & Christen 2011). For the modelling procedure, the resolution and section thickness were set at 5 cm, with a sample size of 12 000.

To examine the variability and magnitude of dust mass accumulation rates during the studied time period, we calculated the MARs for the Velika Vrbica LPS using the following formula:

$$\mathrm{MAR} = \mathrm{SR} \times \mathrm{BD} \times f_{\mathrm{eol}} \quad (3)$$

where SR is the sedimentation rate, BD represents the bulk density, and f_{eol} is the aeolian input content. In this case, we assume that the sediment origin is entirely aeolian (value 1), and the mean bulk density is 1.5 g cm^{-3} (Újvári *et al*. 2010). The presented MAR values in this study lack accompanying uncertainty estimates due to the current absence of a satisfactory method for accurately deriving dust MAR uncertainty from loess deposits (e.g. Újvári *et al*. 2010; Stevens *et al*. 2011; Perić *et al*. 2020, 2022b). The use of simple Gaussian error propagation for luminescence ages may not be appropriate due to uncertainties in bulk density estimates, the effects of postdepositional alterations, and the non-Gaussian or random nature of these uncertainties. Furthermore, even minor variations in the age-depth model can lead to considerable changes in the calculated dust MAR values (Stevens *et al*. 2020). Despite these challenges, it is assumed that MAR estimates are more prone to error in percentage terms than the uncertainty associated with luminescence ages.

Results

Preheat plateau and dose recovery

To determine appropriate preheat conditions for the SAR protocols, we conducted a preheat plateau test (Murray & Wintle 2000) on 15 aliquots of sample 22173. The initial preheat involved temperatures between 180 and 260 °C (in 20 °C increments, with three aliquots per temperature) for 10 s. The test dose preheat (cut-heat) temperatures were consistently set 40 °C lower than the preheat temperatures. The resulting D_e values showed significant scattering, and no clear plateau was observed across the 180–260 °C range (Fig. 3A). As a result, we performed a preheat plateau and dose recovery

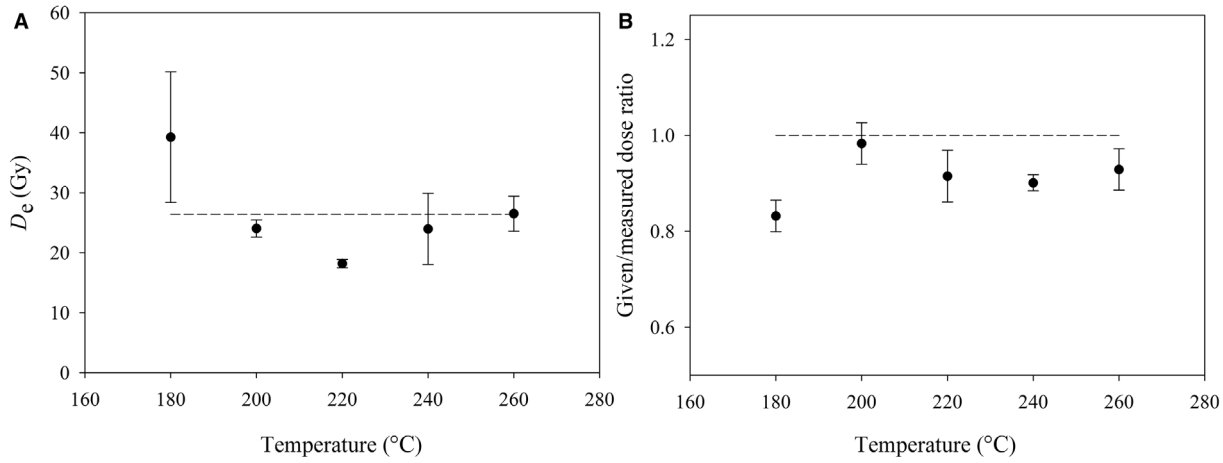

Fig. 3. A. Preheat plateau results for sample 22173, with error bars indicating one standard error. The dashed line represents the mean D_e value calculated across all five temperature points. B. Combined preheat plateau and dose recovery test results for sample 22173, with the dashed line marking the ideal 1:1 dose recovery ratio.

test on another 15 aliquots of sample 22173. Aliquots were initially bleached using blue LEDs for 40 s, followed by a 10 000-s pause. A second bleaching step was then applied with blue LEDs for 40 s, after which a laboratory dose (approximately equivalent to the natural dose) was given. The measurement protocol followed the same procedure as the preheat plateau test, and the resulting dose recovery ratio ranged from 0.8±0.03 at 180 °C to 0.9±0.04 at 260 °C (Fig. 3B). Based on these results, a preheat temperature of 240 °C and a cut-heat temperature of 200 °C were selected for all subsequent measurements. To assess the effectiveness of the selected SAR protocol, a dose recovery test (Murray & Wintle 2003) was conducted on samples 22172, 22174, 22776, 22177 and 22182, with three aliquots analysed per sample. Each aliquot underwent two bleaching treatments with blue LEDs, each lasting 250 s at room temperature, with a 10 000-s pause between treatments. After bleaching, the aliquots were irradiated with beta doses of approximately 8 Gy (sample 22172), 28 Gy (sample 22174), 56 Gy (sample 22176), 85 Gy (sample 22177) and 116 Gy (sample 22182). The measurements were performed using the same protocol as the preheat plateau/dose recovery test. The results, shown in Fig. 4, revealed measured-to-given dose ratios ranging from 0.99±0.05 (sample 22177) to 1.09±0.09 (sample 22176). These results confirm that the chosen SAR protocol accurately measures doses up to at least 115 Gy, prior to any thermal pretreatment.

Quartz OSL properties and D_e

A typical dose–response and decay curve for the Velika Vrbica quartz samples is presented in Fig. 5. The OSL signal was best fitted using a single saturating exponential function. The decay curve exhibited a rapid decrease within the first second. In the inset, the natural and regenerative decay curves are nearly indistinguishable, indicating that the fast component of the OSL signal is dominant. Recuperation was below 5%, and the recycling ratio was close to unity for all accepted aliquots. The D_es for the samples ranged from 7.6±0.4 Gy (sample 22172) to 128.1±6.1 Gy (sample 22182) (Table 1). The samples increase in D_e with depth, with no large jumps or inversions outside uncertainty, with one exception. Between 1.5 and 2 m a large jump in D_e values can be observed: sample 22175 displays a D_e of 23.8±2.7 Gy, while the underlying sample 22176 has a value of 61.0±3.1 Gy. This increase of ∼38 Gy over a 50-cm depth could be an indication of a sedimentation break or erosional event, albeit no obvious eroded layers were observed. Nevertheless, this is not representative of the

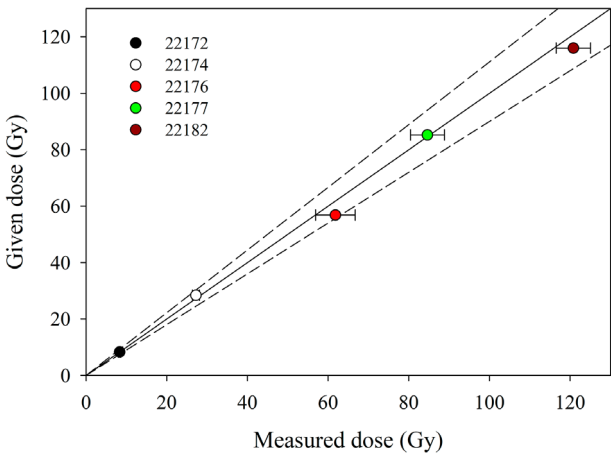

Fig. 4. Dose recovery results for five Velika Vrbica samples. The given irradiation doses were selected to closely approximate the likely equivalent dose of each sample, with test doses set at approximately 20% of the given dose. Three aliquots were analysed per sample. The solid line represents the ideal 1:1 dose recovery ratio, while the dashed lines indicate a 10% deviation from this ideal.

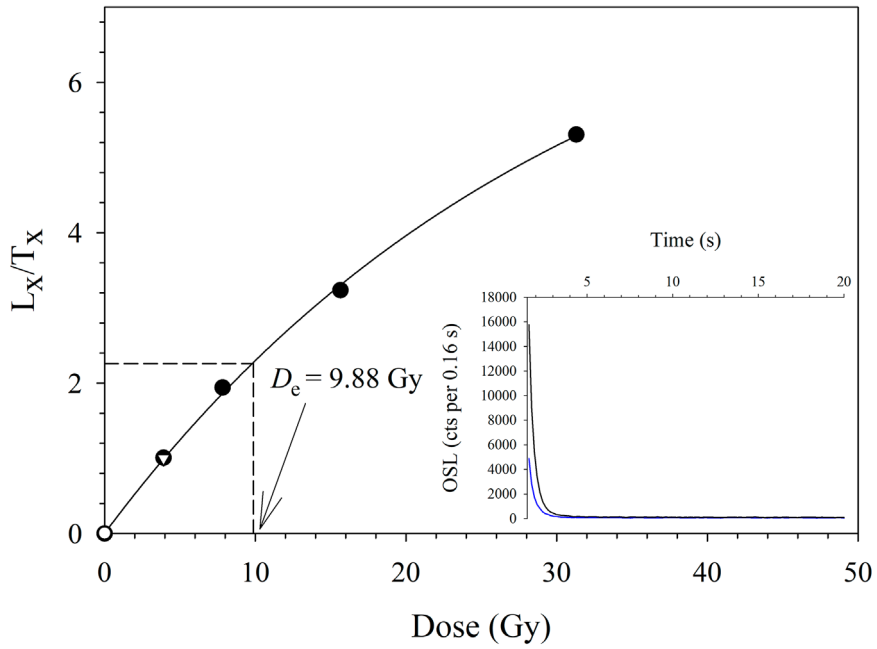

Fig. 5. Representative sensitivity-corrected luminescence dose–response curve for a single aliquot of sample 22172. The dashed line indicates the equivalent dose, while the open circle represents the response to a zero dose (recuperation). An open inverted triangle marks the recycling point. The inset features a typical decay curve of the natural continuous-wave OSL (CW-OSL) signal (solid blue line) compared to a regenerated signal (solid black line) produced by a beta dose approximately corresponding to the equivalent dose.

D_e changes with depth for the rest of the Velika Vrbica LPS.

Wintle and Murray (2006) recommended setting an upper dose threshold of 2 × *D*0 for the fast component of the quartz OSL signal measured through the SAR protocol, corresponding to 86% saturation of the dose–response curve generated in the laboratory. To assess how close the natural, sensitivity-corrected luminescence signals were to laboratory saturation, we calculated the ratio of each natural signal to the average maximum corrected signal produced by a dose of approximately 4000 Gy. This maximum signal was determined from a laboratory dose–response curve (DRC) up to 4000 Gy using sample 22181. The resulting ratios of the sensitivity-corrected natural signal to the laboratory saturation point ranged from 0.07±0.00 (sample 22172) to 0.33±0.03 (sample 22176), with an overall average of 0.19±0.02 (Table S2). Based on this criterion, all calculated OSL ages for the Velika Vrbica LPS were accepted.

Age-depth model and MARs

The luminescence ages display a 100% alignment (within 95% confidence) with the age-depth model constructed by r.bacon (as illustrated in Figs 6, S1). There is a noticeable sensitivity to variations in luminescence age with depth, resulting in a linearly exponential age-depth function (Fig. 6). Furthermore, the model indicates variable MARs, though these variations remain within the error margins of the applied method.

Calculated MARs for the Velika Vrbica LPS are shown in Fig. 7 and Table S3. The MAR values exhibit significant fluctuations throughout the investigated time period, with an average of 171 g m^{-2} a^{-1} where the highest MARs were recorded during MIS 3, averaging 185 g m^{-2} a^{-1}. Peak dust deposition occurred between 38 and 30 ka, with a mean MAR of 196 g m^{-2} a^{-1}. The MIS 2 period displays a lower mean MAR rate (168 g m^{-2} a^{-1}), although the early and late stages recorded relatively high MAR values, as demonstrated in Fig. 7. During mid-MIS 2, a sudden decrease in MAR values was recorded between 17 and 22 ka (mean = 146 g m^{-2} a^{-1}). This suggests that throughout the MIS 2 period, the MARs were much more variable than during MIS 3, with relatively significant variations in their maximum (189 g m^{-2} a^{-1}) and minimum (145 g m^{-2} a^{-1}) values. The Holocene (MIS 1) displayed the lowest mean MAR values, averaging 138 g m^{-2} a^{-1}, however, with a significant variability throughout the period. During the early stage of MIS 1 (12–8 ka), the MARs display an average of 159 g m^{-2} a^{-1}.

This changes relatively rapidly in the Middle Holocene (8–7 ka), where a decrease towards a lower mean MAR (115 g m^{-2} a^{-1}) is observed, with a continuing decline towards the present day. Overall, the MAR trend at Velika Vrbica does not align with the established dust accumulation model, which suggests higher dust accumulation rates during cold glacial phases and lower rates during warmer interglacial stages (Liu 1985; Zhang *et al.* 1999, 2002; Kohfeld & Harrison 2003; Sun & An 2005; Stevens *et al.* 2011). More significant dust input

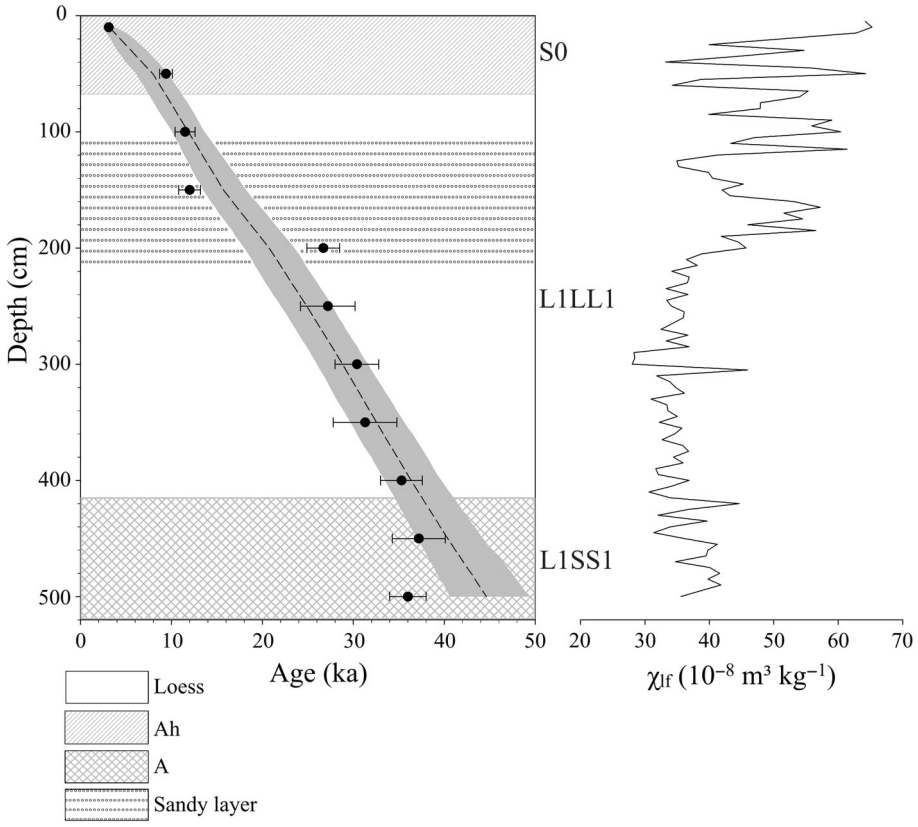

Fig. 6. Age-depth model for the Velika Vrbica LPS. Black solid circles represent the OSL ages, while the grey shaded area indicates the 95% confidence interval for the maximum and minimum age limits. The dashed line depicts the mean age-depth model. These results were generated using the r.bacon age-depth modelling method (details provided in the text). All stratigraphical units are labelled according to the stratigraphical framework proposed by Marković *et al.* (2015). Also presented are the χ_{lf} measurements.

is recorded during the interglacial MIS 3 stage than during the Last Glacial Maximum (LGM).

Magnetic susceptibility (χ_{lf})

The χ_{lf} record (Fig. 6) at the Velika Vrbica LPS from 5 to 3 m shows a generally decreasing trend. At 5-m depth, χ_{lf} is 40×10^{-8} m^3 kg^{-1}, decreasing to a minimum of 28×10^{-8} m^3 kg^{-1} at 2.95 m, which is the lowest observed value in the record. Between 2 and 3 m, χ_{lf} remains relatively stable, averaging 35×10^{-8} m^3 kg^{-1}. At 2.05 m, χ_{lf} increases from 39×10^{-8} to 57×10^{-8} m^3 kg^{-1} at 1.65 m, followed by a drop to the earlier average at 1.25 m. An increase was observed at 0.9-m depth (59×10^{-8} m^3 kg^{-1}) after which χ_{lf} fluctuates between a maximum of 65×10^{-8} m^3 kg^{-1} (0.1 m) and a minimum of 33×10^{-8} m^3 kg^{-1} (0.4 m), with a mean of 52×10^{-8} m^3 kg^{-1}.

Discussion

OSL chronology and age-depth model

The quartz OSL ages calculated for the Velika Vrbica LPS are presented in Fig. 6 as a function of depth. They range from 3.0±0.2 ka for sample 22172 (10-cm depth) to 41.3±2.7 ka for sample 22182 (500-cm depth), indicating that the upper 500 cm of the profile was deposited between the mid stage of MIS 3 and late MIS 1. The ages show a consistent increase to a depth of 350 cm, without any noticeable jumps or decreases (outside uncertainty). However, from 350 to 500 cm, the OSL ages do not display a significant increase, but still remain well within uncertainty limits. This could indicate very high dust deposition during the late stages of MIS 3; however, it might also suggest that the quartz from the Velika Vrbica LPS has reached the threshold for reliable natural dose measurements. In several instances, despite successful dose recovery tests in high dose ranges and the samples being below the $2 \times D0$ limit, natural doses showed no increase, but instead exhibited scattering, and displayed age inversions for samples older than 35 ka (>150 Gy; Buylaert *et al.* 2008). Such issues have been reported globally, including in Romania (Timar-Gabor *et al.* 2011, 2017; Constantin *et al.* 2014), Serbia (Perić *et al.* 2019), and Germany (Zhang *et al.* 2023). Recently, Perić *et al.* (2024) made similar observations at the Kisiljevo LPS, located at the Danube bank (the Iron Gate gorge) 110 km upstream of the Velika Vrbica LPS. From

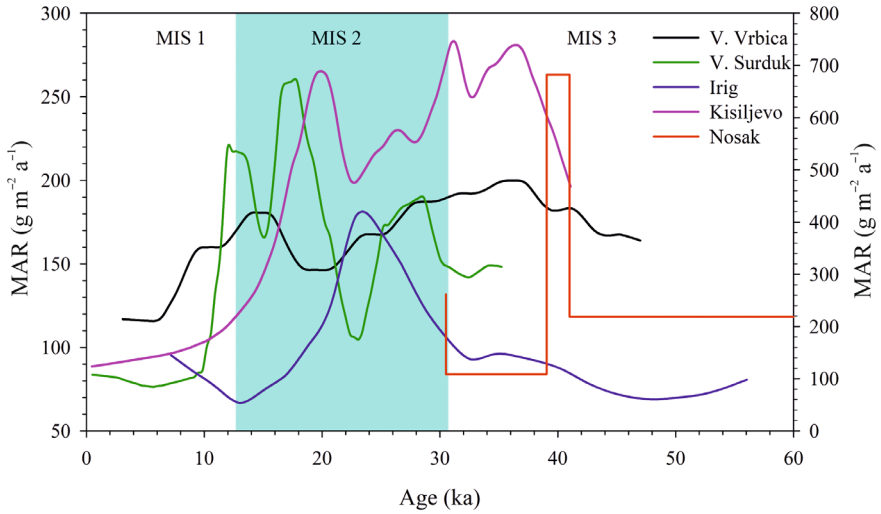

Fig. 7. The dust mass accumulation rates (MARs) for the Velika Vrbica, Veliki Surduk, Irig, Kisiljevo, and Nosak LPSs are shown as functions of age. For Velika Vrbica, Veliki Surduk, Irig, and Kisiljevo, MARs are based on mean ages with 95% confidence intervals and smoothed using the LOESS method (tricube weighting, polynomial regression, SigmaPlot 11.0; sampling proportion = 0.100, polynomial degree = 1). MAR data for the Nosak LPS are from Perić *et al.* (2020), while for Veliki Surduk, Irig and Kisiljevo the data were adopted from Perić *et al.* (2025). The left *y*-axis represents MARs for Velika Vrbica, Veliki Surduk, and Irig, while the right *y*-axis corresponds to Kisiljevo and Nosak.

a depth of 800 cm the ages displayed no significant increase and ranged 32.99±2.59–34.36±1.96 ka, though, as observed at the Velika Vrbica LPS, still remained within uncertainty limits. These ages almost exactly match the threshold of age increase at Velika Vrbica. This may imply that the natural lifetime of quartz OSL signals from the loess sequences in the Middle and Lower Danube Basin is shorter than indicated by laboratory experiments and that the reliable limit for quartz dating in this region is ~35 ka. However, we cannot confirm this without further investigation of older samples from the Velika Vrbica LPS. Nonetheless, the three lowermost ages are consistent (within uncertainty) and remain below 150 Gy, so they are included in the age model.

The L1SS1 palaeosol was dated to ~41–37 ka, which suggests that it developed during the warmer and more humid MIS 3 period (Marković *et al.* 2008). Several studies have reported similar ages for the upper part of the LISS1 pedocomplex in the Vojvodina region across various LPSs. Notable examples include Irig, dated to 27–38 ka (Perić *et al.* 2022b); Surduk, 31.8±3.7 ka (Fuchs *et al.* 2008); Stari Slankamen, 34.4±2.2 ka (Schmidt *et al.* 2010); Crvenka, 38±4 ka (Stevens *et al.* 2011); and Veliki Surduk on the Titel loess plateau 34.2±2.4 ka (Perić *et al.* 2019). These consistent ages across multiple sites underscore a regional climatic pattern during MIS 3, characterized by interstadial conditions conducive to pedogenesis. The increased precipitation and moderate temperatures of this period likely promoted the formation of soils, providing further evidence of MIS 3 as a relatively stable and humid phase amidst the broader oscillations of the Pleistocene climate.

The L1LL1 loess horizon was dated between 35.2±2.4 and 15.0±1.8 ka, covering the late MIS 3 and MIS 2 period. This L1LL1 layer has yielded comparable ages across various LPSs. At the Irig LPS, it was dated to 10.2±0.7 and 24.4±1.7 ka (Perić *et al.* 2022b). Similarly, at the Stari Slankamen LPS, ages of 23.3±1.5 and 23.6±1.4 ka were reported (Schmidt *et al.* 2010; Murray *et al.* 2014). Notably, high-resolution quartz dating at Veliki Surduk revealed ages ranging from 15.6±1.2 to 29.8±5.8 ka (Perić *et al.* 2019). These findings point to variable intensity of loess deposition during periods of cold, arid conditions, interspersed with reduced sedimentation linked to transient climatic variability.

According to the constructed chronology, the sandy layer was deposited between ~32 and 15 ka ago (Figs 2, 6). This sandy layer likely reflects regional climatic and environmental dynamics. Samples 22173 and 22172 recovered from the S0 Holocene soil yielded ages of 9.3±0.8 and 3.0±0.2 ka, respectively. Comparable ages were reported for the Kisiljevo LPS in northeastern Serbia (Perić *et al.* 2024), where the start of Holocene soil formation was dated to 6.7±0.5–0.5±0.05 ka. In the Vojvodina region, similar dates for the S0 layer were determined at multiple loess sections: Crvenka 7.7±0.6 ka (Stevens *et al.* 2011), Veliki Surduk 7.4±0.7 ka (Perić *et al.* 2019) and Stari Slankamen 7.3±0.4 ka (Murray *et al.* 2014), which coincides with our observations. These consistent Holocene soil ages across sites reflect widespread stabilization of the surface under relatively warm and humid conditions, marking a stark contrast to the harsher Pleistocene environments documented in earlier stratigraphical layers.

Magnetic susceptibility and MAR variability

Between 47 and 31 ka, the MARs increased steadily. Field observations revealed that the boundary between MIS 3 and MIS 2 was not clearly distinguishable in the loess complex. During late MIS 3, the palaeoclimate in northern Europe shifted towards glacial conditions. A similar trend is observed in the χ_{lf} record at the Velika Vrbica LPS (Fig. 6). Between 5 and 3 m depth, χ_{lf} values consistently decline, with the exception of an outlier around 420-cm depth. This pattern of decreasing χ_{lf} values is more pronounced at other LPS sites in the neighbouring Vojvodina region during late MIS 3 (Marković *et al.* 2007, 2011, 2018; Vandenberghe *et al.* 2014). The reduction in χ_{lf} values in Vojvodina indicates a change in climatic conditions unfavourable for pedogenesis, a trend also apparent at the Velika Vrbica LPS. As the regional climate shifted towards colder, drier conditions, weathering diminished, leading to greater loess accumulation, as reflected in the increase in MAR values between 47 and 31 ka (Fig. 7).

The evolution of the palaeoenvironmental conditions at Velika Vrbica during late MIS 3 aligns with a similar LPS study from the eastern Wallachian Basin (Obreht *et al.* 2017). The χ_{lf} record at Velika Vrbica (Fig. 6) shows a decrease consistent with trends observed in Vojvodina (Marković *et al.* 2007, 2011, 2018; Vandenberghe *et al.* 2014) and eastern Wallachia (Obreht *et al.* 2017), which documented the development of steppe conditions and increasing continentality between 40 and 27 ka. However, the increase in MAR (mean 193 g m^{-2} a^{-1}) combined with the decreasing trend in χ_{lf} values suggests that the overall climate in the Wallachian Basin was shifting towards the glacial conditions characteristic of MIS 2. This is further evidenced by the fact that loess remained the dominant sediment deposited at the Velika Vrbica LPS during MIS 3. Investigations of the Vlasca and Urluia LPSs in the eastern Wallachian Basin (Obreht *et al.* 2017) reveal a similar trend during late MIS 3. Given that Velika Vrbica is located on the westernmost edge of the basin, this decline in χ_{lf} appears to reflect broader regional climatic changes, rather than a localized phenomenon, indicating a shift towards a colder, more arid climate. The average MAR during MIS 2 (29–12 ka) is 168 g m^{-2} a^{-1} (Fig. 7), which is slightly lower than the values observed during mid/late MIS 3 (45–29 ka: 185 g m^{-2} a^{-1}). Increased aeolian dust activity has been associated with expanded glacial coverage and activity (Smalley 1966). The growth of ice volume and the shift towards glacial conditions are reflected in the increased loess accumulation during the transition to MIS 2. The loess accumulation rates during the MIS 3 to MIS 2 transition support the characterization of a steppe environment in southeastern Europe (Obreht *et al.* 2017), including Velika Vrbica. At ~30 ka, χ_{lf} values remain relatively stable and low, averaging 35×10^{-8} m^3 kg^{-1} (at depths of 2–3 m).

However, an unexpected decline in average MARs is observed during MIS 2. Between 22 and 17 ka, the mean MAR value drops to 146 g m^{-2} a^{-1}. This period coincides with the ~20-ka age jump recorded at depths between 1.5 and 2 m (Fig. 6), overlapping with the position of the sandy layer between 2.2 and 1.1 m. The deposition of coarser material could indicate a different source area or provenance for the sand, distinct from the rest of the section. This suggests that during this period, sediment input was influenced by varying source regions, with the coarser material potentially transported from areas richer in sandy deposits, while the finer sediments reflect more local or consistent sources. Such shifts in sediment provenance highlight changes in transport dynamics and sediment supply during the depositional period. Between ~12 and 20 ka, χ_{lf} values show high variability, with a minimum at 1.25 m and peaks at 1.65 and 0.95 m, corresponding to approximately 15, 19 and 12 ka, respectively. These increasing trends could point to changes in pedogenic conditions or shifts in the depositional regime. Between 1 and 1.5 m (17–13 ka), rapid accumulation occurred (mean MAR = 181 g m^{-2} a^{-1}), while variable χ_{lf} and MAR values can be observed within the sandy layer (1.5–2 m depth). The Holocene is recorded in the upper ~0.90 m, comprising two units: S0 and the upper part of L1. Loess accumulation during the Early Holocene led to ~0.20 m of L1 deposition continuing into the postglacial period. Our age-depth model results indicate that the transition from loess to soil occurred around 10 ka, suggesting ~2000 years of loess accumulation during the Early Holocene. This observation aligns with findings by Constantin *et al.* (2021), who demonstrated that dust accumulation continued into the Holocene at multiple loess sites in southeastern Europe, China, and the US. Their luminescence chronology provides direct evidence that sedimentation and pedogenesis can occur simultaneously, contributing to an accretional component in Holocene soil formation. This process has important implications for interpreting magnetic susceptibility and other palaeoenvironmental proxies, as it suggests that loess accumulation persisted even during soil development. Furthermore, their modelled accumulation rates for the Holocene soils, ranging from 2 to 9 cm ka^{-1} across different regions, support the interpretation of continued loess deposition during the Early Holocene at Velika Vrbica. Similar evidence of ongoing dust deposition into the Holocene has been documented in other parts of the Wallachian Basin. At Lunca, Romania, 28 cm of loess was deposited during MIS 1 (Constantin *et al.* 2015), while delayed pedogenesis during the same period was observed in the eastern Wallachian Basin (Timar-Gabor *et al.* 2011). A similar lag in soil formation was also observed west of Velika Vrbica in the neighbouring Vojvodina region (Marković *et al.* 2014). These records of dust deposition and the delayed onset of Holocene soils across the Lower Danube Basin point to a com-

mon climatic trend. Velika Vrbica and other LPS sites in the region show evidence of a variable Early Holocene climate, with a lack of soil formation suggesting the environment was less warm and humid than during the Middle to Late Holocene. Therefore, the transition between the glacial conditions of late MIS 2 and the warm, humid climate of the Holocene was not abrupt. Continued dust accumulation during the Early Holocene may be the result of the site's proximity to the Danube River. This persistent loess deposition may also explain the variability in χ_{lf} values in the upper 70 cm of the section. Additionally, anthropogenic activities, such as agriculture, could have caused disturbances in the S0 unit.

The χ_{lf} values in the upper 0.7 m (S0) exhibit significant fluctuations (Fig. 6). This trend is comparable to the values recorded in the topsoil samples in Vojvodina (Radaković *et al*. 2019). In the northeastern Chernozem soils of the Bačka Loess Plateau, low χ_{lf} values have been linked to the input of coarser grains, such as quartz and silts. Quartz grains, which are iron-deficient, have low χ_{lf} values. The proximity of the Velika Vrbica LPS to the Danube River, along with surrounding alluvial and sandy deposits, suggests that short-lived wind events may have deposited nearby grains into the Chernozem S0 unit, leading to the χ_{lf} variations recorded during the Holocene (Fig. 6). Despite these fluctuations, the Middle to Late Holocene exhibits the highest mean χ_{lf} values of any period.

Generally, the MAR pattern at the Velika Vrbica LPS diverges from the conventional models of loess formation; however, it does not present an isolated case, as similar dust deposition trends have been observed at other LPSs in the wider region. At the Nosak LPS in northeastern Serbia (Perić *et al*. 2020), where the MIS 7–MIS 3 period was dated, a distinct MAR peak during MIS 3, with very high values (682 g m^{-2} a^{-1}), was observed, albeit occurring earlier in the phase than at Velika Vrbica (42–36 ka). Recent analyses at the neighbouring Kisiljevo LPS (Perić *et al*. 2024) reveal a comparable pattern (Fig. 7). Although the entire MIS 3 interval is not preserved at Kisiljevo, two distinct dust peaks, dated to 38–33 and 32–30 ka, are evident, with maximum MAR values centred at approximately 31 ka. This closely aligns with the timing of peak dustiness at Velika Vrbica. While high MIS 3 MAR values could be influenced by dating uncertainties, the consistent observation of similar trends at multiple sites in proximity to the Danube suggests they likely represent genuine episodes of intensified atmospheric dust activity. In contrast, LPS records from the Vojvodina region, such as Irig (Perić *et al*. 2022b) and Veliki Surduk LPSs (Perić *et al*. 2019), exhibit a more uniform MAR distribution during MIS 3, without pronounced peaks (Fig. 7). The distinctive MAR patterns observed at Velika Vrbica, Kisiljevo and Nosak compared to the Vojvodina sites may result from localized or regional environmental factors. These could include increased dust transport rates, enhanced deposition efficiency, elevated palaeowind intensities (Gavrilov *et al*. 2018), or the closer proximity of these sites to the Danube River. Moreover, local patterns of vegetation, soil humidity, and topography could have influenced the observed MAR variability. Vegetation cover can impact dust trapping efficiency, while soil moisture levels may affect surface stability and dust availability. Topographical features could further modulate wind flow and dust deposition patterns at a micro-regional scale. These findings emphasize the importance of site-specific factors in controlling loess deposition and provide new insights into the spatial variability of dust flux during MIS 3. However, the apparent increase in sedimentation rates during MIS 3 compared to MIS 2 could, at least in part, be an artefact if the ages older than 35 ka are affected by uncertainties. Potential limitations in age control for this interval may lead to an overestimation of sedimentation rates, influencing interpretations of dust flux variability. Refining age models through additional independent chronological constraints would help assess the robustness of these trends and improve confidence in the reconstructed depositional history.

Regional comparison of environmental magnetic records

The frequency-dependent magnetic susceptibility (χlf) values from the Serbian LPSs at Velika Vrbica and Irig, along with the Romanian LPSs at Urluia and Vlasca (Obreht *et al*. 2017), are presented in Fig. 8. A comparative analysis of these records reveals a distinct pattern: while the Velika Vrbica, Urluia, and Vlasca sequences exhibit strong similarities, the Irig LPS stands apart with a markedly different trend. This coherence among the Velika Vrbica, Urluia, and Vlasca records suggests a regionally consistent climatic signal, reflecting broader palaeoenvironmental conditions within the Lower Danube Basin (Obreht *et al*. 2017). The presence of these shared trends across spatially distinct sites reinforces the interpretation of a common climatic trajectory governing loess accumulation and pedogenesis in this part of southeastern Europe. The high variability observed in the χ_{lf} records from Velika Vrbica, Urluia, and Vlasca is indicative of pronounced fluctuations in environmental conditions, likely driven by alternating phases of dust deposition and pedogenic processes. This variability aligns with well-documented climate oscillations that characterize the Late Pleistocene and suggests that these sites experienced similar shifts in aeolian input, moisture availability, and pedogenic intensity. In contrast, the Irig LPS presents a relatively smooth χ_{lf} profile, lacking the pronounced peaks, declines, and recoveries observed in the other records. This fundamental difference implies that the Irig site was influenced by a distinct set of environmental factors that modulated its susceptibility signal differently than in the Lower Danube Basin. A plausible explanation for this discrepancy lies in the regional and local controls on sedimentation and pedo-

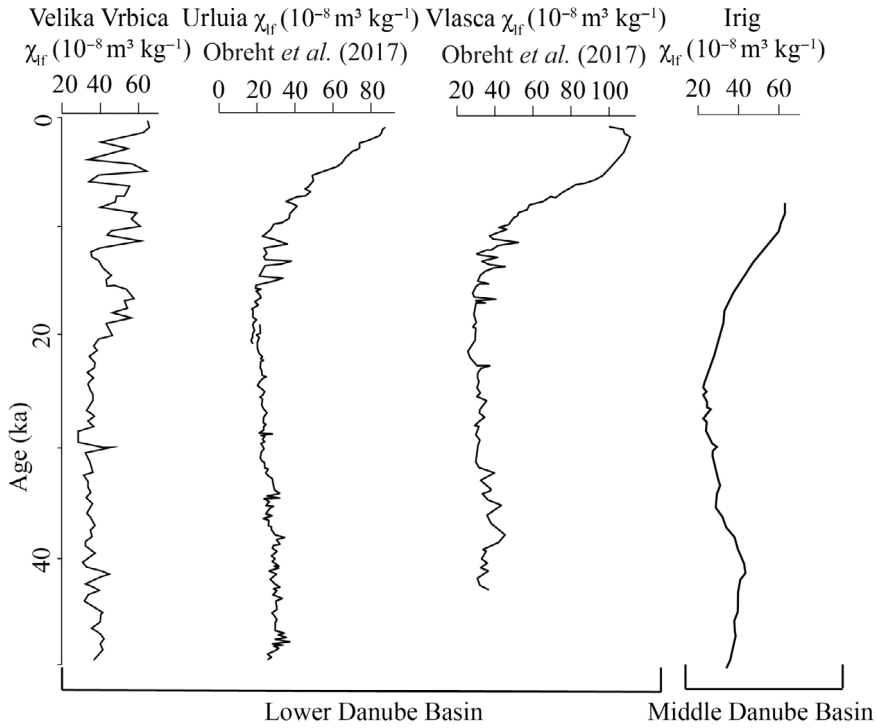

Fig. 8. χ_{lf} (10^{-8} m^3 kg^{-1}) records from LPSs in the Middle (Irig – Perić *et al.* 2022b) and Lower Danube (Velika Vrbica – this study; Urluia and Vlasca – Obreht *et al.* 2017) Basins. Age models extend to ~45 000 years, enabling regional comparisons of dust accumulation and pedogenic intensity across the Middle and Lower Danube Basins.

genesis (e.g. Fenn *et al.* 2021). Differences in dust provenance, predominant wind directions, and geomorphological settings may have played a significant role in shaping the χ_{lf} signal at each site. Velika Vrbica, Urluia, and Vlasca are located closer to major dust sources, such as the Danube flood-plain, which likely contributed to higher dust accumulation rates and, consequently, greater variability in their χ_{lf} records. Additionally, these sites may have been more directly exposed to climatic fluctuations that influenced soil formation processes, further enhancing the variability observed in their records. In contrast, the Irig site appears to have been influenced by a more stable depositional environment, potentially characterized by a more consistent sediment source or lower susceptibility to short-term climatic perturbations. Another striking feature of the Velika Vrbica record is its divergence from the characteristic plateau-like shape of the χ_{lf} signal commonly associated with MIS 3 in the Vojvodina region, as exemplified by the Irig LPS. Instead of displaying a relatively stable magnetic susceptibility trend during MIS 3, Velika Vrbica exhibits more pronounced fluctuations, suggesting a different climatic or depositional regime. This deviation from the expected pattern raises important questions about the factors controlling loess accumulation and pedogenesis at this site. One possible explanation is that Velika Vrbica was subjected to stronger climatic variability, leading to more dynamic shifts between loess deposition and soil formation. Furthermore, the Lateglacial segment of the Velika Vrbica χ_{lf} record also differs from the typical patterns observed in the Middle Danube Basin loess sequences of Serbia. While many loess sites in this region display relatively subdued variations in χ_{lf} during this period, Velika Vrbica stands out with a more fluctuating susceptibility signal. This suggests that local environmental conditions, such as variations in moisture availability, vegetation cover, or postdepositional processes, may have played a significant role in shaping the χ_{lf} record at this site. In summary, the comparative analysis of χ_{lf} records from the Velika Vrbica, Urluia, Vlasca, and Irig loess sections reveals important regional and site-specific differences in loess accumulation and pedogenesis. The strong similarities between Velika Vrbica, Urluia, and Vlasca point to a regionally coherent climatic signal in the Lower Danube Basin, reinforcing the interpretation of a shared climatic history across these sites. In contrast, the distinctive nature of the Irig record suggests that different environmental controls, such as sediment source, prevailing wind patterns, and geomorphology, played a more dominant role in shaping its susceptibility signal. The deviations observed in the Velika Vrbica record, particularly in the MIS 3 and Lateglacial intervals, highlight the complexity of palaeoenvironmental reconstructions and emphasize the need for further investigations into the specific factors driving these variations.

Conclusions

The Velika Vrbica LPS provides a high-resolution archive of palaeoenvironmental changes spanning MIS 3 to MIS 1, offering critical insights into the climatic and environmental evolution of southeastern Europe during the late Quaternary. Crucially, the established OSL chronology highlights consistent loess deposition from ~41 to 3 ka, capturing the transition from glacial to interglacial conditions. It is also notable that significant accumulation occurred during MIS 3 and MIS 2, with variations in low field magnetic susceptibility (χ_{lf}) and mass accumulation rates (MARs) reflecting the complex interplay between aeolian activity, pedogenesis, and regional environmental factors. These findings reveal a nuanced response to climatic transitions, with periods of enhanced dust deposition coinciding with both colder glacial phases and warmer interglacial conditions. This dual pattern challenges conventional models of loess formation, which traditionally associate increased dust activity with glacial climates characterized by stronger winds and aridity. In particular, the heightened dust accumulation observed during MIS 3 interstadial phases underscores the need to reconsider the interactions between global climatic drivers and local environmental processes, such as proximity to major sediment sources like the Danube River, regional wind patterns, and variations in sediment trapping efficiency. These inconsistencies may be influenced by site-specific factors or regional climatic conditions that deviate from broader trends, emphasizing the importance of localized studies within a global context. Additionally, the possibility that higher sedimentation rates during MIS 3 compared to MIS 2 may be an artefact due to potential age uncertainties for sediments older than 35 ka should be considered. Further chronological refinements would be necessary to fully assess the robustness of this pattern. The comparison with Lower Danube Basin records reveals both synchronies and regional disparities, suggesting that local factors, including topography and sediment supply, modulated the broader climatic signals. This highlights the complexity of loess formation processes and the need for site-specific analyses to unravel these dynamics fully. Overall, this study underscores the value of loess archives as exceptional records of past environmental changes. The Velika Vrbica LPS not only improves our understanding of the palaeoclimate of southeastern Europe but also provides critical perspectives on the mechanisms driving loess formation and dust deposition. Future research integrating higher-resolution dating, extended stratigraphical coverage, and comparative studies across adjacent regions will be crucial to resolving these discrepancies and advancing our knowledge of the interplay between regional environments and global climate systems. This work ultimately reaffirms the role of terrestrial archives in refining our understanding of Earth's climatic history and the processes shaping its landscapes.

Acknowledgements. – This study was supported by the Royal Physiographic Society in Lund (grant nos 42788 and 43046). MGR is grateful for a L'Oréal-UNESCO For Women in Science award. SBM is grateful to the Silesian Technical University for the guest professorship position awarded by the Rector's Commission for Awards and Proquality Programmes. This research was also supported by the Project F-178 of the Serbian Academy of Sciences and Arts and by the Science Fund of the Republic of Serbia, #17807, The Loess Plateau Margins: Towards Innovative Sustainable Conservation – LAMINATION. The authors gratefully acknowledge the financial support of the Ministry of Science, Technological Development and Innovation of the Republic of Serbia (grant nos 451-03-137/2025-03/200125 and 451-03-136/2025-03/200125). This research was conducted within the Lu^2D^2 (The Lund Luminescence centre for Dating and Dosimetry) infrastructure. We would also like to thank the anonymous reviewer 1 as well as Professor J. Vandenberghe for their constructive comments and suggestions, which helped improve the quality of this study.

Author contributions. – ZMP: conceptualization; investigation; funding acquisition; writing – original draft; methodology; validation; visualization; writing – review and editing; software; formal analysis; project administration; data curation; supervision; resources. CSR: conceptualization; investigation; methodology; validation; writing – review and editing; formal analysis. WT: investigation; methodology; writing – review and editing; formal analysis. MGR: investigation; methodology; visualization; writing – review and editing. PK: investigation; writing – review and editing. HA: investigation; methodology; writing – review and editing; software; formal analysis. SBM: investigation; methodology; writing – review and editing; formal analysis; supervision.

Data availability statement. – The data that support the findings of this study are available from the corresponding author upon reasonable request.

References

Antoine, P., Rousseau, D. D., Fuchs, M., Hatté, C., Gauthier, C., Marković, S. B., Jovanović, M., Gaudenyi, T., Moine, O. & Rossignol, J. 2009: High-resolution record of the last climatic cycle in the southern Carpathian Basin (Surduk, Vojvodina, Serbia). *Quaternary International 198*, 19–36. https://doi.org/10.1016/J.QUAINT.2008.12.008.

Avramov, V. I., Jordanova, D., Hoffmann, V. & Roesler, W. 2006: The role of dust source area and pedogenesis in three loess-palaeosol sections from North Bulgaria: A mineral magnetic study. *Studia Geophysica et Geodaetica 50*, 259–282. https://doi.org/10.1007/S11200-006-0015-Y

Blaauw, M. & Christen, J. A. 2011: Flexible paleoclimate age-depth models using an autoregressive gamma process. *Bayesian Analysis 6* (3), 457–474. https://doi.org/10.1214/11-BA618.

Bøtter-Jensen, L., Andersen, C. E., Duller, G. A. T. & Murray, A. S. 2003: Developments in radiation, stimulation and observation facilities in luminescence measurements. *Radiation Measurements 37*, 535–541. https://doi.org/10.1016/S1350-4487(03)00020-9.

Brennan, B. J., Lyons, R. G. & Phillips, S. W. 1991: Attenuation of alpha particle track dose for spherical grains. *International Journal of Radiation Applications and Instrumentation. Part D. Nuclear Tracks and Radiation Measurements 18* (1–2), 249–253. https://doi.org/10.1016/1359-0189(91)90119-3.

Buylaert, J. P., Murray, A. S., Vandenberghe, D., Vriend, M., De Corte, F. & van den Haute, P. 2008: Optical dating of Chinese loess using sand-sized quartz: establishing a time frame for late Pleistocene climate changes in the western part of the Chinese loess plateau. *Quaternary Geochronology 3*, 99–113. https://doi.org/10.1016/j.quageo.2007.05.003.

Constantin, D., Begy, R., Vasiliniuc, S., Panaiotu, C., Necula, C., Codrea, V. & Timar-Gabor, A. 2014: High-resolution OSL dating of the Costineşti section (Dobrogea, SE Romania) using fine and coarse quartz. *Quaternary International 334–335*, 20–29. https://doi.org/10.1016/J.QUAINT.2013.06.016.

Constantin, D., Cameniță, A., Panaiotu, C., Necula, C., Codrea, V. & Timar-Gabor, A. 2015: Fine and coarse-quartz SAR-OSL dating of Last Glacial loess in Southern Romania. *Quaternary International 357*, 33–43. https://doi.org/10.1016/j.quaint.2014.07.052.

Constantin, D., Mason, J. A., Veres, D., Hambach, U., Panaiotu, C., Zeeden, C., Zhou, L., Marković, S. B., Gerasimenko, N., Avram, A., Tecsa, V., Groza-Sacaciu, S. M., del Valle Villalonga, L., Begy, R. & Timar-Gabor, A. 2021: OSL-dating of the Pleistocene-Holocene climatic transition in loess from China, Europe and North America, and evidence for accretionary pedogenesis. *Earth-Science Reviews 221*, 103769. https://doi.org/10.1016/j.earscirev.2021.103769.

Constantin, D., Veres, D., Panaiotu, C., Anechitei-Deacu, V., Groza, S. M., Begy, R., Kelemen, S., Buylaert, J. P., Hambach, U., Marković, S. B., Gerasimenko, N. & Timar-Gabor, A. 2019: Luminescence age constraints on the Pleistocene-Holocene transition recorded in loess sequences across SE Europe. *Quaternary Geochronology 49*, 71–77. https://doi.org/10.1016/J.QUAGEO.2018.07.011.

Duller, G. A. T. 2015: The Analyst software package for luminescence data: overview and recent improvements. *Ancient TL 33*, 35–42.

Durcan, J. A., King, G. E. & Duller, G. A. T. 2015: DRAC: Dose Rate and Age Calculator for trapped charge dating. *Quaternary Geochronology 28*, 54–61. https://doi.org/10.1016/j.quageo.2015.03.012.

Fenn, K., Thomas, D. S. G., Durcan, J. A., Millar, I. L., Veres, D., Piermattei, A. & Lane, C. S. 2021: A tale of two signals: global and local influences on the Late Pleistocene loess sequences in Bulgarian Lower Danube. *Quaternary Science Reviews 274*, 107264. https://doi.org/10.1016/j.quascirev.2021.107264.

Fuchs, M., Rousseau, D. D., Antoine, P., Hatté, C., Gauthier, C., Marković, S. & Zoeller, L. 2008: Chronology of the Last Climatic Cycle (Upper Pleistocene) of the Surduk loess sequence, Vojvodina, Serbia. *Boreas 37*, 66–73. https://doi.org/10.1111/J.1502-3885.2007.00012.X.

Gavrilov, M. B., Marković, S. B., Schaetzl, R. J., Tošić, I., Zeeden, C., Obreht, I., Sipos, G., Ruman, A., Putniković, S., Emunds, K., Perić, Z., Hambach, U. & Lehmkuhl, F. 2018: Prevailing surface winds in Northern Serbia in the recent and past time periods; modern- and past dust deposition. *Aeolian Research 31*, 117–129. https://doi.org/10.1016/J.AEOLIA.2017.07.008.

Guérin, G., Mercier, N. & Adamiec, G. 2011: Dose-rate conversion factors: update. *Ancient TL 29*, 5–8.

Guérin, G., Mercier, N., Nathan, R., Adamiec, G. & Lefrais, Y. 2012: On the use of the infinite matrix assumption and associated concepts: a critical review. *Radiation Measurements 47*, 778–785. https://doi.org/10.1016/j.radmeas.2012.04.004.

Hansen, V., Murray, A., Buylaert, J.-P., Yeo, E.-Y. & Thomsen, K. 2015: A new irradiated quartz for beta source calibration. *Radiation Measurements 81*, 123–127. https://doi.org/10.1016/j.radmeas.2015.02.017.

Hrouda, F. & Ježek, J. 2014: Frequency-dependent AMS of rocks: a tool for the investigation of the fabric of ultrafine magnetic particles. *Tectonophysics 629*, 27–38. https://doi.org/10.1016/j.tecto.2014.01.040.

Hrouda, F. & Pokorný, J. 2011: Extremely high demands for measurement accuracy in precise determination of frequency-dependent magnetic susceptibility of rocks and soils. *Studia Geophysica et Geodaetica 55*, 667–681. https://doi.org/10.1007/s11200-010-0079-6.

Hrouda, F., Pokorný, J., Ježek, J. & Chadima, M. 2013: Out-of-phase magnetic susceptibility of rocks and soils: a rapid tool for magnetic granulometry. *Geophysical Journal International 194* (1), 170–181. https://doi.org/10.1093/gji/ggt097.

Jordanova, D., Laag, C., Jordanova, N., Lagroix, F., Georgieva, B., Ishlyamski, D. & Guyodo, Y. 2022a: A detailed magnetic record of Pleistocene climate and distal ash dispersal during the last 800 kyrs—the Suhia Kladenetz quarry loess-paleosol sequence near Pleven (Bulgaria). *Global and Planetary Change 214*, 103840. https://doi.org/10.1016/j.gloplacha.2022.103840.

Jordanova, D., Simon, Q., Balescu, S., Jordanova, N., Ishlyamski, D., Georgieva, B., Bourlès, D. L., Duvivier, A. & Cornu, S. 2022b: Environmental changes in southeastern Europe over the last 450 ka: magnetic and pedologic study of a loess-paleosol profile from Kaolinovo (Bulgaria). *Quaternary Science Reviews 292*, 107671. https://doi.org/10.1016/j.quascirev.2022.107671.

Kohfeld, K. E. & Harrison, S. P. 2003: Glacial-interglacial changes in dust deposition on the Chinese Loess Plateau. *Quaternary Science Reviews 22* (18-19), 1859–1878. https://doi.org/10.1016/S0277-3791(03)00166-5.

Laag, C., Hambach, U., Zeeden, C., Lagroix, F., Guyodo, Y., Veres, D., Jovanović, M. & Marković, S. B. 2021: A detailed paleoclimate proxy record for the Middle Danube Basin over the last 430 kyr: A rock magnetic and colorimetric study of the Zemun loess-paleosol sequence. *Frontiers in Earth Science 9*, 600086. https://doi.org/10.3389/feart.2021.600086

Lehmkuhl, F., Nett, J. J., Pötter, S., Schulte, P., Sprafke, T., Jary, Z., Antoine, P., Wacha, L., Wolf, D., Zerboni, A., Hošek, J., Marković, S. B., Obreht, I., Sümegi, P., Veres, D., Zeeden, C., Boemke, B., Schaubert, V., Viehweger, J. & Hambach, U. 2021: Loess landscapes of Europe – mapping, geomorphology, and zonal differentiation. *Earth-Science Reviews 215*, 103496. https://doi.org/10.1016/j.earscirev.2020.103496.

Liu, T. 1985: *Loess and the Environment*. 18–28. China Ocean Press, Beijing.

Marković, S. B., Bokhorst, M. P., Vandenberghe, J., McCoy, W. D., Oches, E. A., Hambach, U., Gaudenyi, T., Jovanović, M., Zöller, L., Stevens, T. & Machallet, B. 2008: Late Pleistocene loess-palaeosol sequences in the Vojvodina region, north Serbia. *Journal of Quaternary Science 23*, 73–84. https://doi.org/10.1002/JQS.1124

Marković, S. B., Fitzsimmons, K. E., Sprafke, T., Gavrilović, D., Smalley, I. J., Jović, V., Svirčev, Z., Gavrilov, M. B. & Bešlin, M. 2016: The history of Danube loess research. *Quaternary International 399*, 86–99. https://doi.org/10.1016/j.quaint.2015.09.071.

Marković, S. B., Hambach, U., Stevens, T., Kukla, G. J., Heller, F., McCoy, W. D., Oches, E. A., Buggle, B. & Zöller, L. 2011: The last million years recorded at the Stari Slankamen (Northern Serbia) loess-palaeosol sequence: revised chronostratigraphy and long-term environmental trends. *Quaternary Science Reviews 30* (9-10), 1142–1154. https://doi.org/10.1016/J.QUASCIREV.2011.02.004.

Marković, S. B., Oches, E. A., McCoy, W. D., Frechen, M. & Gaudenyi, T. 2007: Malacological and sedimentological evidence for "warm" glacial climate from the Irig loess sequence, Vojvodina, Serbia. *Geochemistry, Geophysics, Geosystems 8*, Q09008. https://doi.org/10.1029/2006GC001565.

Marković, S. B., Oches, E. A., Perić, Z. M., Gaudenyi, T., Jovanović, M., Sipos, G., Thiel, C., Buylaert, J.-P., Savić, S., Mccoy, W. D., Radaković, M. G., Marković, R. S. & Gavrilov, M. B. 2021: The Požarevac loess-paleosol sequence: a record of increased aridity in the south-eastern margin of the Carpathian Basin during the last 350 ka. *Journal of Quaternary Science 36*, 1436–1447. https://doi.org/10.1002/jqs.3327

Marković, S. B., Stevens, T., Kukla, G. J., Hambach, U., Fitzsimmons, K. E., Gibbard, P., Buggle, B., Zech, M., Guo, Z., Hao, Q., Wu, H., O'Hara Dhand, K., Smalley, I. J., Újvári, G., Sümegi, P., Timar-Gabor, A., Veres, D., Sirocko, F., Vasiljević, D. A., Jary, Z. & Svirčev, Z. 2015: Danube loess stratigraphy—towards a pan-European loess stratigraphic model. *Earth-Science Reviews 148*, 228–258. https://doi.org/10.1016/J.EARSCIREV.2015.06.005.

Marković, S. B., Sümegi, P., Stevens, T., Schaetzl, R. J., Obreht, I., Chu, W., Buggle, B., Zech, M., Zech, R., Zeeden, C., Gavrilov, M. B., Perić, Z., Svirčev, Z. & Lehmkuhl, F. 2018: The Crvenka loess-paleosol sequence: a record of continuous grassland domination in the southern Carpathian Basin during the Late Pleistocene. *Palaeogeography, Palaeoclimatology, Palaeoecology 509*, 33–46. https://doi.org/10.1016/J.PALAEO.2018.03.019.

Marković, S. B., Timar-Gabor, A., Stevens, T., Hambach, U., Popov, D., Tomić, N., Obreht, I., Jovanović, M., Lehmkuhl, F., Kels, H., Marković, R. & Gavrilov, M. B. 2014: Environmental dynamics and luminescence chronology from the Orlovat loess-palaeosol sequence (Vojvodina, northern Serbia). *Journal of Quaternary Science 29*, 189–199. https://doi.org/10.1002/JQS.2693.

Murray, A. S. & Wintle, A. G. 2000: Luminescence dating of quartz using an improved single-aliquot regenerative-dose protocol. *Radiation Measurements 32*, 57–73. https://doi.org/10.1016/S1350-4487(99)00253-X.

Murray, A. S. & Wintle, A. G. 2003: The single aliquot regenerative dose protocol: potential for improvements in reliability. *Radiation Measurements 37* (4–5), 377–381. https://doi.org/10.1016/S1350-4487(03)00053-2.

Murray, A. S., Schmidt, E. D., Stevens, T., Buylaert, J. P., Marković, S. B., Tsukamoto, S. & Frechen, M. 2014: Dating Middle Pleistocene loess from Stari Slankamen (Vojvodina, Serbia)—limitations imposed by the saturation behaviour of an elevated temperature IRSL signal. *Catena 117*, 34–42. https://doi.org/10.1016/J.CATENA.2013.06.029.

Murray, A., Marten, R., Johnston, A. & Martin, P. 2005: Analysis for naturally occuring radionuclides at environmental concentrations by gamma spectrometry. *Journal of Radioanalytical and Nuclear Chemistry Articles 115* (2), 263–288. https://doi.org/10.1007/bf02037443.

Obreht, I., Hambach, U., Veres, D., Zeeden, C., Bösken, J., Stevens, T., Marković, S. B., Klasen, N., Brill, D., Burow, C. & Lehmkuhl, F. 2017: Shift of large-scale atmospheric systems over Europe during late MIS 3 and implications for Modern Human dispersal. *Scientific Reports 7*, 5848. https://doi.org/10.1038/s41598-017-06285-x.

Obreht, I., Zeeden, C., Schulte, P., Hambach, U., Eckmeier, E., Timar-Gabor, A. & Lehmkuhl, F. 2015: Aeolian dynamics at the Orlovat loess–paleosol sequence, northern Serbia, based on detailed textural and geochemical evidence. *Aeolian Research 18*, 69–81. https://doi.org/10.1016/J.AEOLIA.2015.06.004

Perić, Z. M., Marković, S. B., Avram, A., Timar-Gabor, A., Zeeden, C., Nett, J. J., Fischer, P., Fitzsimmons, K. E. & Gavrilov, M. B. 2022a: Initial quartz OSL and dust mass accumulation rate investigation of the Kisiljevo loess sequence in north-eastern Serbia. *Quaternary International 620*, 13–23. https://doi.org/10.1016/J.QUAINT.2020.10.040.

Perić, Z. M., Marković, S. B., Sipos, G., Gavrilov, M. B., Thiel, C., Zeeden, C. & Murray, A. S. 2020: A post-IR IRSL chronology and dust mass accumulation rates of the Nosak loess-palaeosol sequence in northeastern Serbia. *Boreas 49*, 841–857. https://doi.org/10.1111/bor.12459.

Perić, Z. M., Radaković, M. G., Marković, R. S. & Marković, S. B. 2025: A synthesis of luminescence and C dated dust mass accumulation rates for loess-palaeosol sequences from the Middle Danube Basin. *Boreas 54*, 179–201. https://doi.org/10.1111/bor.12696.

Perić, Z. M., Ryan, C., Alexanderson, H. & Marković, S. B. 2024: Revised OSL chronology of the Kisiljevo loess-palaeosol sequence: new insight into the dust flux in the eastern Carpathian Basin during MIS 3–MIS1. *Quaternary International 698*, 39–48. https://doi.org/10.1016/j.quaint.2024.06.006.

Perić, Z. M., Stevens, T., Obreht, I., Hambach, U., Lehmkuhl, F. & Marković, S. B. 2022b: Detailed luminescence dating of dust mass accumulation rates over the last two glacial–interglacial cycles from the Irig loess-palaeosol sequence, Carpathian Basin. *Global and Planetary Change 215*, 103895. https://doi.org/10.1016/j.gloplacha.2022.103895.

Perić, Z., Lagerbäck Adolphi, E., Stevens, T., Újvári, G., Zeeden, C., Buylaert, J. P., Marković, S. B., Hambach, U., Fischer, P., Schmidt, C., Schulte, P., Huayu, L., Shuangwen, Y., Lehmkuhl, F., Obreht, I., Veres, D., Thiel, C., Frechen, M., Jain, M., Vött, A., Zöller, L. & Gavrilov, M. B. 2019: Quartz OSL dating of late quaternary Chinese and Serbian loess: a cross Eurasian comparison of dust mass accumulation rates. *Quaternary International 502*, 30–44. https://doi.org/10.1016/J.QUAINT.2018.01.010.

Pokorný, J., Pokorný, P., Suza, P. & Hrouda, F. 2011: A multi-function Kappabridge for high precision measurement of the AMS and the variations of magnetic susceptibility with field, temperature and frequency. *In* Petrovský, E., Ivers, D., Harinarayana, T. & Herrero-Bervera, E. (eds.): *The Earth's Magnetic Interior*, 293–301. Springer, Dordrecht. https://doi.org/10.1007/978-94-007-0323-0_20.

Prescott, J. R. & Hutton, J. T. 1994: Cosmic ray contributions to dose rates for luminescence and ESR dating: large depths and long-term time variations. *Radiation Measurements 23*, 497–500. https://doi.org/10.1016/1350-4487(94)90086-8.

Radaković, M. G., Gavrilov, M. B., Hambach, U., Schaetzl, R. J., Tošić, I., Ninkov, J., Vasin, J. & Marković, S. B. 2019: Quantitative relationships between climate and magnetic susceptibility of soils on the Bačka Loess Plateau (Vojvodina, Serbia). *Quaternary International 502*, 85–94. https://doi.org/10.1016/j.quaint.2018.04.040.

Roberts, H. M. & Wintle, A. G. 2001: Equivalent dose determinations for polymineralic fine-grains using the SAR protocol: application to a Holocene sequence of the Chinese Loess Plateau. *Quaternary Science Reviews 20* (5–9), 859–863. https://doi.org/10.1016/S0277-3791(00)00051-2.

Schaetzl, R. J., Bettis, E. A., Crouvi, O., Fitzsimmons, K. E., Grimley, D. A., Hambach, U., Lehmkuhl, F., Marković, S. B., Mason, J. A., Owczarek, P., Roberts, H. M., Rousseau, D. D., Stevens, T., Vandenberghe, J., Zárate, M., Veres, D., Yang, S., Zech, M., Conroy, J. L., Dave, A. K., Faust, D., Hao, Q., Obreht, I., Prud'homme, C., Smalley, I., Tripaldi, A., Zeeden, C. & Zech, R. 2018: Approaches and challenges to the study of loess—introduction to the LoessFest special issue. *Quaternary Research 89* (3), 563–618. https://doi.org/10.1017/QUA.2018.15.

Schmid, S. M., Fügenschuh, B., Kounov, A., Maţenco, L., Nievergelt, P., Oberhänsli, R., Pleuger, J., Schefer, S., Schuster, R., Tomljenović, B., Ustaszewski, K. & van Hinsbergen, D. J. J. 2020: Tectonic units of the Alpine collision zone between Eastern Alps and western Turkey. *Gondwana Research 78*, 308–374. https://doi.org/10.1016/j.gr.2019.07.005.

Schmidt, E. D., Machalett, B., Marković, S. B., Tsukamoto, S. & Frechen, M. 2010: Luminescence chronology of the upper part of the Stari Slankamen loess sequence (Vojvodina, Serbia). *Quaternary Geochronology 5*, 137–142. https://doi.org/10.1016/J.QUAGEO.2009.09.006.

Smalley, I. J. 1966: The properties of glacial loess and the formation of loess deposits. *Journal of Sedimentary Research 36*, 669–676. https://doi.org/10.1306/74D7153C-2B21-11D7-8648000102C1865D.

Stevens, T., Marković, S. B., Zech, M., Hambach, U. & Sümegi, P. 2011: Dust deposition and climate in the Carpathian Basin over an independently dated last glacial–interglacial cycle. *Quaternary Science Reviews 30*, 662–681. https://doi.org/10.1016/j.quascirev.2010.12.011.

Stevens, T., Sechi, D., Bradák, B., Orbe, R., Baykal, Y., Cossu, G., Tziavaras, C., Andreucci, S. & Pascucci, V. 2020: Abrupt last glacial dust fall over southeast England associated with dynamics of the British-Irish ice sheet. *Quaternary Science Reviews 250*, 106641. https://doi.org/10.1016/J.QUASCIREV.2020.106641.

Sun, Y. & An, Z. 2005: Late Pliocene-Pleistocene changes in mass accumulation rates of eolian deposits on the central Chinese Loess Plateau. *Journal of Geophysical Research: Atmospheres 110* (D23), D23101. https://doi.org/10.1029/2005JD006064.

Timar-Gabor, A., Buylaert, J.-P., Guralnik, B., Trandafir-Antohi, O., Constantin, D., Anechitei-Deacu, V., Jain, M., Murray, A. S., Porat, N., Hao, Q. & Wintle, A. G. 2017: On the importance of grain size in luminescence dating using quartz. *Radiation Measurements 106*, 464–471. https://doi.org/10.1016/j.radmeas.2017.01.009.

Timar-Gabor, A., Vandenberghe, D. A. G., Vasiliniuc, S., Panaoitu, C. E., Panaiotu, C. G., Dimofte, D. & Cosma, C. 2011: Optical dating of Romanian loess: a comparison between silt-sized and sand-sized quartz. *Quaternary International 240*, 62–70. https://doi.org/10.1016/j.quaint.2010.10.007.

Újvári, G., Kovács, J., Varga, G., Raucsik, B. & Marković, S. B. 2010: Dust flux estimates for the Last Glacial Period in East Central Europe based on terrestrial records of loess deposits: a review. *Quaternary Science Reviews 29* (23-24), 3157–3166. https://doi.org/10.1016/J.QUASCIREV.2010.07.005.

Vandenberghe, J., Markovič, S. B., Jovanovič, M. & Hambach, U. 2014: Site-specific variability of loess and palaeosols (Ruma, Vojvodina, northern Serbia). *Quaternary International 334–335*, 86–93. https://doi.org/10.1016/j.quaint.2013.10.036.

Wintle, A. G. & Murray, A. S. 2006: A review of quartz optically stimulated luminescence characteristics and their relevance in single-aliquot regeneration dating protocols. *Radiation Measurements 41*, 369–391. https://doi.org/10.1016/J.RADMEAS.2005.11.001.

Zhang, J., Zolitschka, B., Hogrefe, I., Tsukamoto, S., Binot, F. & Frechen, M. 2023: High-resolution luminescence-dated sediment record for the last two glacial-interglacial cycles from Rodderberg, Germany. *EarthArXiv*. https://eartharxiv.org/repository/view/6325/.

Zhang, X. Y., Arimoto, R. & An, Z. S. 1999: Glacial and interglacial patterns for Asian dust transport. *Quaternary Science Reviews 18* (6), 811–819. https://doi.org/10.1016/s0277-3791(98)00028-6.

Zhang, X. Y., Lu, H. Y., Arimoto, R. & Gong, S. 2002: Atmospheric dust loadings and their relationship to rapid oscillations of the Asian winter monsoon climate: two 250-kyr loess records. *Earth and Planetary Science Letters 202* (3–4), 637–643. https://doi.org/10.1016/s0012-821x(02)00797-5.

Supporting Information

Additional Supporting Information to this article is available at http://www.boreas.dk.

Fig. S1 r.bacon (Blaauw & Christen 2011) generated age-depth Bayesian model for the Velika Vrbica LPS. The results are based on millions of Monte Carlo iterations yielding a mean confidence of 95%. Top panel: time series of the log-posterior for the sub-sampled MCMC (left), prior (green) and posterior (grey) for accumulation rates. Mean confidence ranges 6147 a, min. 1138 a at 10-cm depth, max. 8776 a at 500-cm depth. 100% of the dates overlap with the age-depth model (95% ranges).

Table S1 Summary of the measured equivalent doses along with the performance parameters of the SAR protocol for the quartz from the Velika Vrbica LPS. *n* represents the number of aliquots averaged for D_e calculations. The errors represent 1 standard error.

Table S2 Summary of the saturation level calculation for all measured quartz samples from the Velika Vrbica LPS.

Table S3 Summary of the r.bacon modelled minimum (min.) maximum (max.), median (med.), and mean ages for the Velika Vrbica LPS according to depth. Also shown are the calculated dust mass accumulation rates expressed in g m^{-2} a^{-1}.